Preferential crystal orientation etching of GaN nanopillars in Cl2 plasma

Lucas Jaloustre, Valentin Ackermann, Saron Sales de Mello, Sébastien Labau, Camille Petit-Etienne, Erwine Pargon

Preferential crystal orientation etching of GaN nanopillars in Cl_2 plasma

Jaloustre Lucas [a], Ackermann Valentin [a], Sales De Mello Saron [a], Labau Sébastien [a], Petit-Etienne Camille [a], Pargon Erwine [a*]

[a] *Univ. Grenoble Alpes, CNRS, CEA/LETI-Minatec, Grenoble INP, Institute of Engineering and Management University Grenoble Alpes, LTM, Grenoble F-38054, France*

* *erwine.pargon@cea.fr, Univ. Grenoble Alpes, CNRS, LTM, 17 rue des Martyrs, 38054 Cedex 09 Grenoble, France*

Abstract

The ability to fabricate organized, dense arrays of GaN nanostructures with high aspect ratios is of great interest for improving light extraction and absorption in optoelectronic devices, such as light-emitting diodes (LEDs) and Lasers.
However, achieving this requires a patterning method that allows for the fabrication of GaN nanostructures with a controlled final shape and specific crystallographic facets. Our study shows that a top-down approach combining lithography and Cl_2-based plasma etching processes offers the possibility of anisotropically transferring a pattern while revealing smooth nonpolar facets.
Although GaN etching in Cl_2 is driven by ion-enhanced chemical etching mechanisms, the chemical component is very strong, and Cl_2 plasma leads to preferential crystallographic orientation etching of GaN. The mechanisms that drive facet formation are very similar to those involved in wet KOH etching. The etching ability of a specific crystallographic plane by chlorine atoms depends on the planar density and the N dangling bonds present on the plane. Predictably, GaN crystallographic planes will be etched in Cl_2 plasmas as follows: a-type semipolar > m-type semipolar planes > a nonpolar plane > m polar planes > c polar planes. Crystallographic etching usually reveals the slowest etching planes, meaning the m-planes. However, consistently with the wet mechanisms, our study shows that the final revealed plane in Cl_2 plasma will strongly depend on the surface curvature: in concave surfaces, fast-etch facets persist, while in convex surfaces, slow-etch facets persist. Consequently, Cl_2 plasma etching of pillars (convex surfaces) will result in a-type facets, while etching of holes (concave surfaces) result in m-type facets.

1. Introduction

Currently, GaN-based light emitting diodes (LEDs) are the leading technology for solid-state lighting [1]. Compared to conventional thin film LEDs, GaN-based nanorods [2–4] offer several potential advantages, including a reduction in crystalline defect density [5] and improved light extraction efficiency due to their non-planar geometry [6].

Most promisingly, core-shell light-emitting devices are expected to be a breakthrough development in solid-state lighting [6–9]. In this approach, the emissive quantum wells are grown on the entire sidewalls of the nanowire, which are closely aligned with nonpolar planes. In addition to the advantages of the 3D geometry, this architecture provides: i) an increase in the emissive surface area compared to a planar structure by a factor of about four times the nanowire aspect ratio [2], and ii) an improvement in internal quantum efficiency (IQE) by avoiding piezoelectric polarization and associated electric fields (Quantum-confined Stark effect) through regrowth on high-quality nonpolar facets [10–13].
Therefore, the ability to fabricate organized, dense arrays of GaN nanowires with high aspect ratio is of great interest for the next generation of devices, such as core-shell light emitting diodes.
The array of GaN nanowires can be obtained through a bottom-up approach (using molecular beam epitaxy [14,15] or metal-organic vapor phase epitaxy [8,9] self-organized growth) or a top-down approach (a combination of lithography and plasma etching steps) [16–20].

The advantage of the top-down approach is that it offers more flexibility in creating arrays of nanowires with different shapes, dimensions, and densities on a wafer scale. However, plasma patterning is known to cause damage and rough surfaces, which prevent high-quality surface regrowth [21,22] while the regrowth of the quantum wells on the nanowire sidewalls for core/shell emitting structures is favored if m-oriented facets are present.
One of the greatest challenges in patterning high aspect ratio GaN nanowires is achieving high GaN-to-mask etch selectivity while maintaining high-quality etched surfaces. Most studies addressing this etch selectivity issue use Ni-based hard masks obtained by lift-off lithography, since they offer high selectivity for deep GaN etching (>15) [16–18,23]. However, for certain applications, the use of metal masks may not be desired due to potential contamination and hard mask roughness issues [22]. For industrial applications, the use of dielectric masks is preferred. One group demonstrated the feasibility of fabricating ultra-deep etching of GaN pillars with a SiO_2 dielectric mask and GaN/SiO_2 selectivities over 20 under several chemically driven etch conditions [19,20,24].
Regarding plasma chemistries, all studies converge on the point that chlorine plasmas (pure Cl_2 or Ar/Cl_2) are the most suitable for deeply etching GaN with high etch rates (200-500 nm/min) [16–20,23], and minimal surface defects and roughness when compared to plasmas with BCl_3 or $SiCl_4$ additives [25–27]. Another interesting aspect of chlorine-based plasmas for etching GaN pillars is that they apparently lead to preferential crystallographic orientation. Several authors have highlighted that under certain conditions, nonpolar a-plane facets appear during GaN pillar etching in Cl_2 [19,20,28]. However, the mechanisms responsible for these facets are still unclear. Gaining a better understanding of GaN faceting during plasma etching could have significant implications for a wide range of optoelectronics and photonics applications. For instance, when targeting core-shell LED emitters, the presence of nonpolar m-planes is preferred after pillar patterning to facilitate the regrowth of quantum wells by Metalorganic vapour-phase epitaxy (MOVPE) on the sidewalls.

In this study, we bring some new understanding into the mechanisms that lead to crystalline facet formation during GaN etching in Cl_2 plasma. To address this issue, we patterned arrays of high aspect ratio GaN nanowires (AR > 10) with SiO_2 hard masks and using a Cl_2 plasma process. Well-defined hard mask shapes (hexagonal or circular) whose edges are perfectly aligned with the m or a crystalline planes of the underneath GaN are used to evaluate if the shape of the mask with respect to the crystallographic GaN plane could have a role in the Cl_2 plasma etching mechanisms. Our results show that the mechanisms that drive facet formation in Cl_2 plasma are very similar to those involved in wet KOH etching.

2. Experimental setup

2.1. Sample preparation

Micro-pillars are fabricated using a commercial 4-inch c-sapphire substrate, on which a 4 µm-thick (0001) Ga-polar GaN layer is grown. An 800 nm-thick SiO_2 hard mask (HM) is deposited on the GaN layer using Plasma Enhanced Chemical Vapor Deposition (PECVD). Then, we dice the wafer into small coupons measuring 1.1 by 0.7 mm. An electron-sensitive resist (ma-N 2410) with a thickness of 800 nm is spin-coated on the coupons and patterned using electron beam lithography (EBL). The patterns consist of dots with hexagonal or circular shapes, with diameters (inscribed circle) ranging from 0.25 to 2 µm, and three different densities (space between dots of 2 µm, 5 µm or 15 µm, also referred to as dense, semi-dense, and isolated) (cf. Fig. 1). The hexagonal dots have two orientations corresponding respectively to a-planes and the m-planes of GaN with ±1 ° precision (cf. Fig. 1-b).

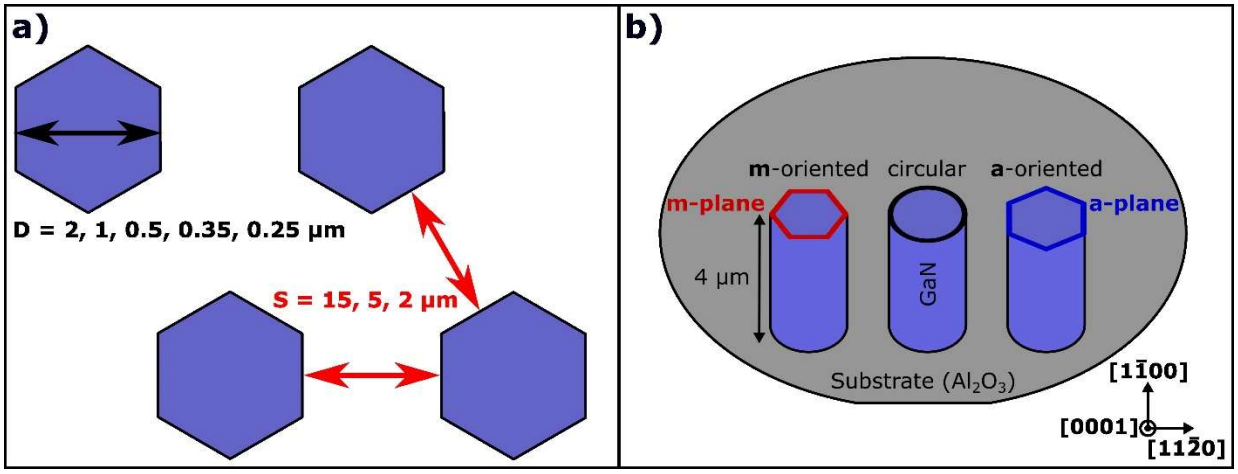

Figure 1. a) Design of the lithography pattern where D is the diameter of the dots varying from 0.25 to 2µm and S the space between the dots varying from 2 to 15 µm. b) Shapes of the dots, could be hexagonal oriented with a- or m- planes of the GaN or circular.

2.2. Plasma etching reactor and processes

The etching experiments were conducted using a Centura 5200 etch platform from Applied Materials, which comprises three plasma reactors [29]. First, we thermally glued GaN samples onto a 200 mm carrier wafer using silicone-free thermal paste (Type 1977-DP) from Techspray. Then, we opened the SiO_2 hard mask using Magnetically Enhanced Reactive Ion Etching (MERIE) with an $Ar/C_4F_8/O_2$ plasma. This plasma process ensures a SiO_2/resist etch selectivity of 1.7. Finally, we stripped the resist using an O_2 plasma, with a SiO_2 carrier wafer being used for both these steps.

For the GaN etching step, an Inductively Coupled Plasma (ICP) reactor (Decoupled Plasma Source, DPS, from Applied Materials) is used with a Cl_2 plasma (190 sccm), a pressure of 25 mTorr, a source power of 400 W, and a bias power of 140 W (corresponding to a VDC of -450 V). The chuck temperature is maintained at 55 °C, and a SiN carrier wafer is used for this step. The GaN etching process is monitored in real-time and stopped at the end of the process using an endpoint system that utilizes interferometry with a Xenon lamp providing wavelengths from 200 to 800 nm (EyeD from Verity instrument). After GaN etching, buffered oxide etch (BOE) wet solution is used to remove the hard mask layer.

2.3. Characterization

A FEI Helios-450s Focused Ion Beam Scanning Transmission Electron Microscopy (FIB-STEM) is used to image the pillars after the different steps of dry and wet etching.

In-situ Energy Dispersive X-ray spectroscopy (EDX) analysis has been performed on thin lamellae prepared using the dual beam system. An in-situ micromanipulator is used to extract the lamella and place it on a copper grid for the thinning process and observations. The following observation parameters were used: 3 kV and 50 pA for Scanning Electron Microscopy (SEM) images to avoid charging effects, 29 kV and 50 pA for STEM images, and 20 kV and 1.6 nA for EDX analysis.

3. Experimental results and discussion

3.1. Hard mask opening optimization

The first part of the experimental section aims to draw attention to the importance of controlling the hard mask opening step for GaN pillar etching in chlorine plasma. In the MERIE reactor, there is no endpoint detection system, so the process is stopped based on time. The process time was previously estimated by calculating the etch rates of SiO_2 film deposited on Si and exposed to the HM opening process. A process time of 170 s was estimated to etch the 800 nm thick HM layer. The HM opening is then followed by the O_2 stripping plasma in the MERIE reactor. As shown in Fig. 2-a, the HM profiles obtained are quite satisfactory

and could be used to etch the GaN pillars at first sight. However, the GaN pillars etched with this HM opening strategy have some strange defects, such as a collar appearing in the middle of the profile, regardless of the Cl_2 plasma conditions investigated (cf. Fig. 2-b). Further investigations into the hard mask opening strategy helped us better understand the reason for these defects.

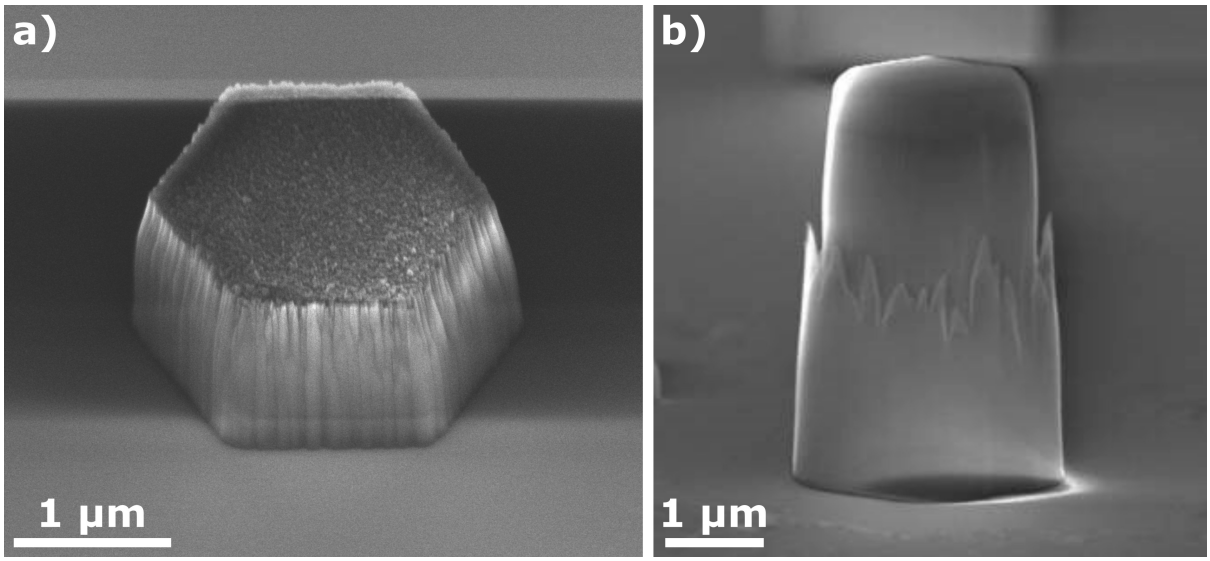

Figure 2. a) Hard mask profile after the hard mask opening step. b) Pillar after the GaN etching in Cl_2 plasma presenting a collar.

FIB-STEM and EDX analyses were carried out after the HM opening and stripping step, revealing a consumption of the GaN layer of approximately 50 nm, accompanied by some redeposition on the HM sidewalls (cf. Fig. 3-a). Further investigations indicated that two mechanisms were involved: i) the HM opening step was too long and not selective on GaN, inducing GaN consumption of around 30 nm and a first layer of redeposits, ii) the energetic O_2 stripping of the MERIE reactor added another 20 nm of GaN consumption and redeposits. EDX analyses shown in Fig. 3-b revealed the presence of Ga in the deposition, indicating that the GaN was sputtered on the HM sidewalls by line of sight deposition. Based on those observations, the HM opening processing time was properly adjusted to avoid GaN consumption. Moreover, as the ion energy is hardly controllable in the MERIE reactor, the O_2 stripping step was achieved in the ICP reactor using an O_2 plasma with no bias applied to the wafer. With those two optimized steps, a small GaN consumption of 2 nm and redeposition of 4 nm was observed (cf. Fig. 4-a). Using the optimized hard mask processing, the GaN pillars were then etched with the Cl_2 plasma. Fig. 4-b clearly shows no collar. The thick Ga-based deposition layers formed on the HM sidewalls with the non-optimized HM patterning were clearly identified as responsible for the collar. At the beginning of the Cl_2 process, they acted as a masking material. But, as they were less resistant to the Cl_2 plasma than the SiO_2 HM, they were rapidly consumed and introduced a micromasking all around the pillar, creating the collar.

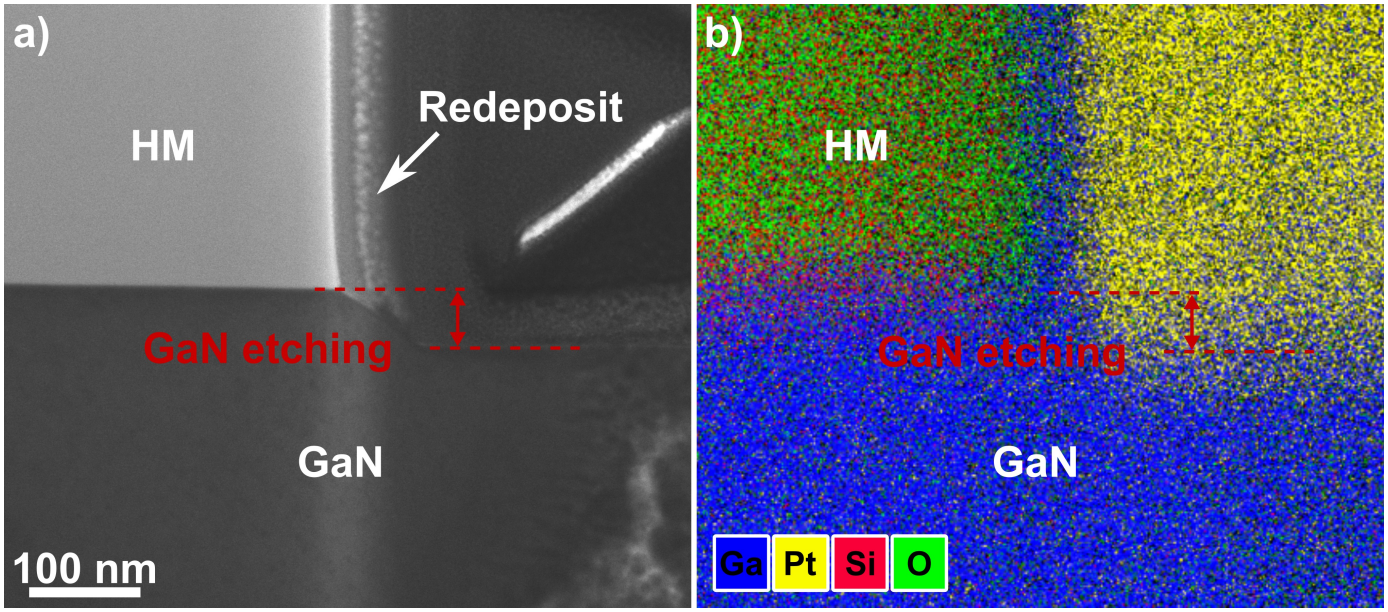

Figure 3. Lamella collected after the initial hard mask opening and stripping steps. a) STEM image showing the damage in the GaN layer and the redeposits on the hard mask sidewalls. b) EDX analysis (20 kV, 1.6 nA) showing the Ga rich composition of the redeposits.

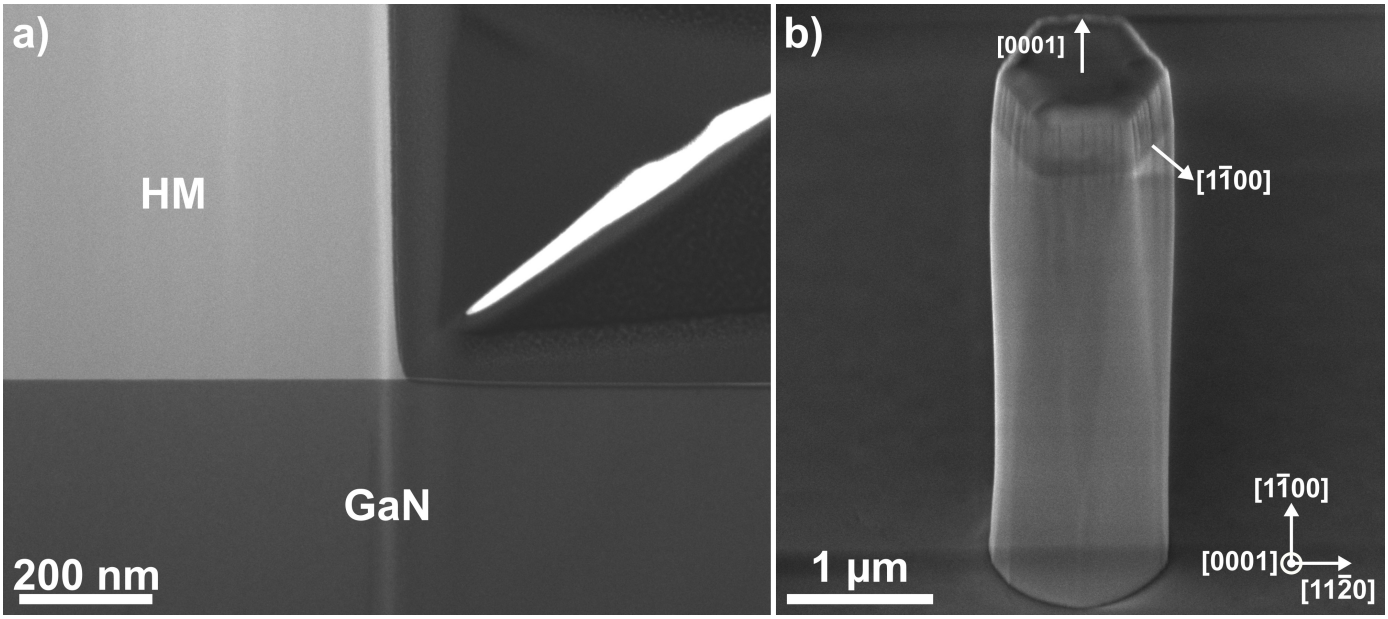

Figure 4. Improvement of the hard mask opening and stripping steps illustrated by: a) STEM image of a lamella collected after the hard mask opening and the stripping showing no GaN damaged and redeposits. b) SEM image of pillar after the GaN etching showing the absence of collar.

3.2. GaN etching in Cl_2 plasma

Fig. 5 shows the profiles of pillars with diameters of 0.25 µm, 0.5 µm, and 2 µm, which were etched with the m-oriented hexagonal hard mask using our optimized Cl_2 plasma process before and after BOE. The GaN etch rate for this process is around 145 nm/min and the GaN/SiO_2 etch selectivity is 10, which is in the same range as other studies [19,20,24].

After the GaN etching step (cf. Fig. 5-a to c), the pillar profiles obtained are highly anisotropic. Sidewall striations are visible at the top of the pillars, which were initially present in the hard mask (cf. Fig. 2-a) and

transferred into the GaN. About 1 µm below the hard mask, the pillars exhibit a bulging part. This phenomenon is present in all pillars but is more noticeable in the isolated ones. At the bottom of the pillars, hexagonal facets appear.

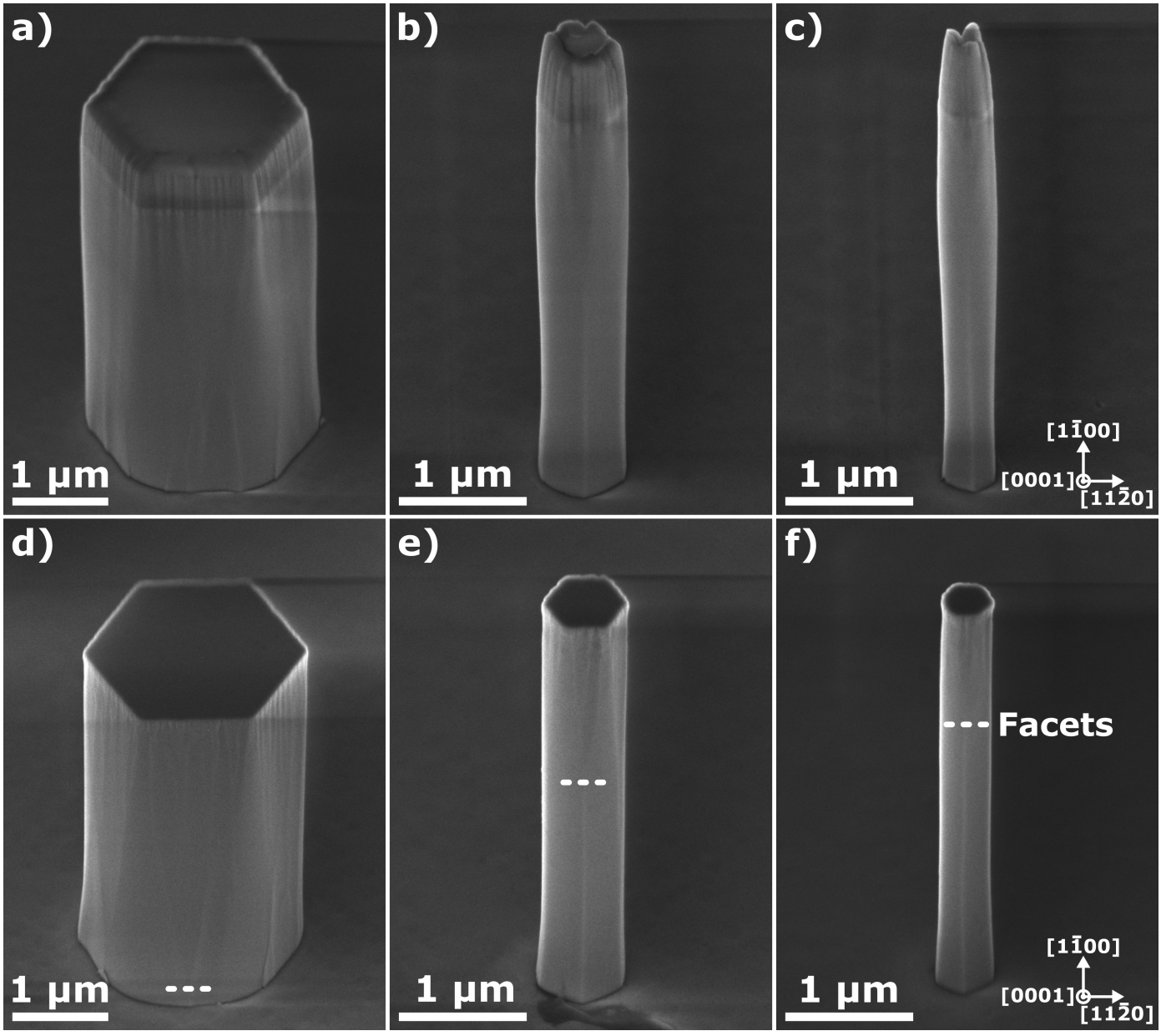

Figure 5. SEM images of GaN pillars with m-oriented hexagonal hard mask of 2 – 0.5 – 0.25 µm diameter in tiled view (45° with a rotation of 30°) after etching and before BOE: a), b), c) and after BOE treatment: d), e), f). The dashed line represents the height reached by the a-oriented facets.

After a 2-hour BOE treatment (cf. Fig. 5-d to f), the pillar profiles became more anisotropic, and the bulging part located 1 µm below the hard mask was removed. To estimate the thickness of the redeposit that formed the bulging area, we compared pillar diameters taken 1 µm below the hard mask before and after BOE. Fig. 6 shows the redeposit thickness for various pillar diameters and spacings. Two trends are apparent from these curves: 1) the thickness of the redeposits slightly increases as the pillar diameter decreases, but this trend could be due to measurement accuracy. 2) More redeposits (around 50 nm) are found on isolated pillars compared to dense ones (around 20 nm). FIB-STEM and EDX analyses performed after GaN etching on 1 µm-diameter isolated pillars indicate that those deposits are Si-based etch byproducts (cf. Fig. 7-c to

g). This indicates that the deposition comes from the etching of the SiN carrier wafer and that the SiN etch byproducts redeposit from the plasma on the pillar sidewalls [24]. Since the collection angle of neutral depositing species is greater in isolated than dense pillars, thicker deposits are observed for isolated pillars (cf. Fig. 6). The deposit thickness is at its maximum at about 1 µm below the hard mask (measured at 37 nm for isolated 1 µm-diameter pillar) (cf. Fig. 7-b), as it is sputtered at the top of the pillar, and the pillar bottom is exposed to plasma for a shorter time. The formation of Si-based deposits on the pillar sidewalls results in a diameter increase at the bottom of the pillar compared to the initial HM imprint. The thicker the deposit, the more significant the diameter increase [30]. Therefore, the diameter of the pillars increases by around 50, 70, and 80 nm, respectively, for dense, semi-dense, and isolated arrays.

The BOE treatment reveals the etching striations present at the top of the pillars and the smooth hexagonal facets at the bottom of the pillars. The facets are fully hexagonal for small diameter pillars of 0.5 µm or lower (cf. Fig. 5-e and f), partially formed for 1 µm pillars but not present on the 2 µm pillars (cf. Fig. 5-d). The orientation of these facets is always the same and corresponds to the a-plane of the GaN, indicating that the process is crystallographic orientation-dependent and not aligned with the m-oriented hard mask.

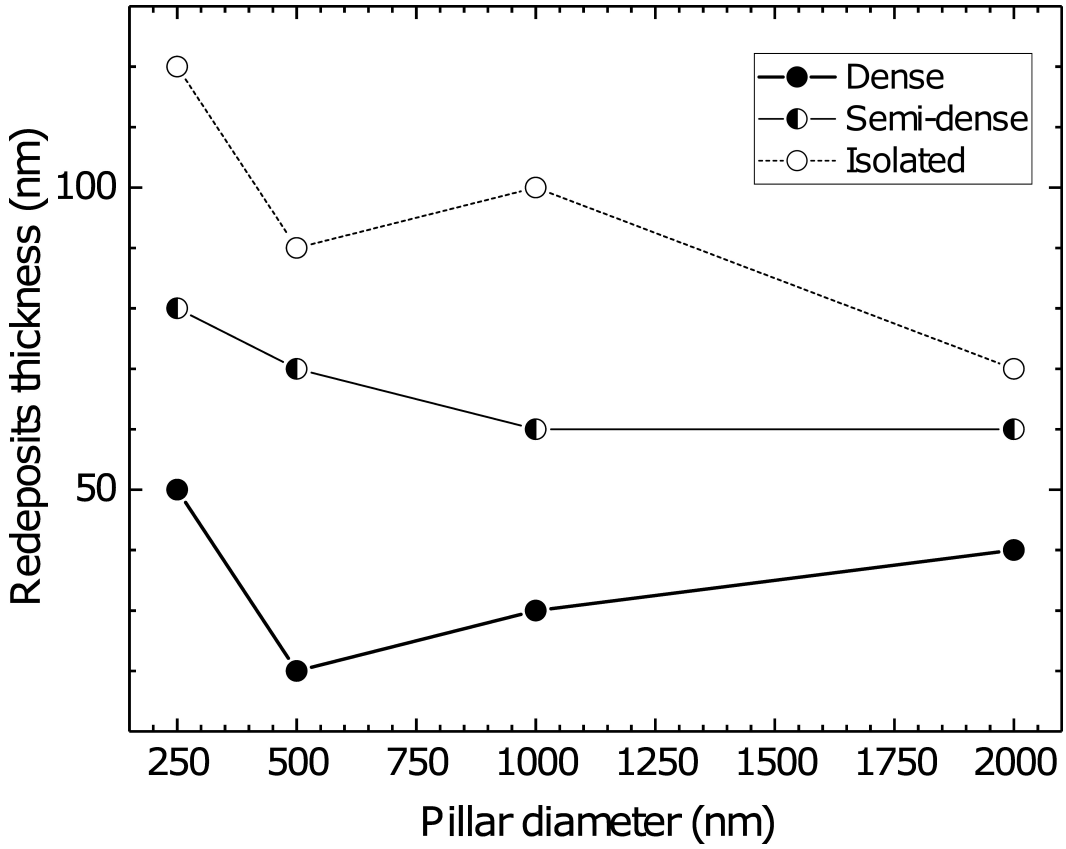

Figure 6. Thickness of redeposits measured on pillars of different diameters and different pitches. Redeposit thickness is calculated from tilted view SEM images by making the difference of pillar diameter before and after BOE divided by two.

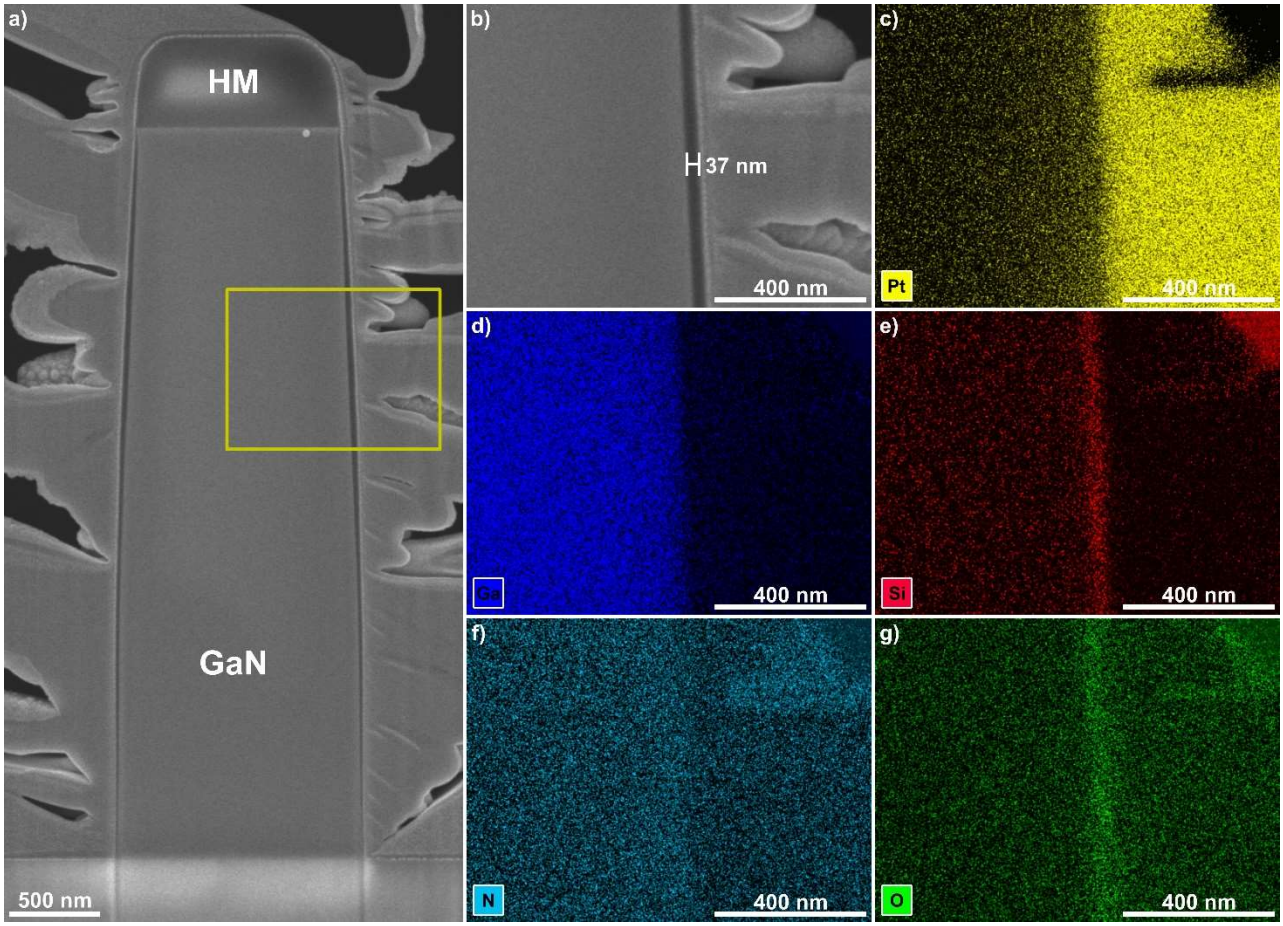

Figure 7. FIB-STEM lamella and EDX analysis of post-etching redeposits. a) SEM cross section of a 1 µm-diameter pillar, the yellow box corresponds to the area analysed by EDX; c), d), e), f) and g) are the EDX mapping of the chemical elements present in the analysed area of the sidewalls shown in b).

A similar Cl_2 plasma process was used to pattern GaN pillars with a-oriented and circular hard masks to investigate the influence of hard mask shape on faceting formation (cf. Fig. 8). SEM images of the pillars after BOE confirm that plasma etching leads to the formation of facets corresponding to GaN a-planes regardless of the initial HM shape. Facet formation is facilitated for smaller pillars and when the initial hard mask facets are aligned with the GaN a-plane. Thus, with an a-oriented HM, pillars of all diameters show well-defined a-plane facets from the base to the top (cf. Fig. 8-c and f). In contrast, m-oriented HM results in a-facets only for pillars with a diameter of 1 µm or less, and the facets remain located at the base of the pillars (Fig. 8-a and d). Circular HM exhibits an intermediate behaviour where facets are visible at the base of all pillars and extend higher than for m-oriented HM but do not reach the top of the pillars (Fig. 8b and e).

The appearance of a-plane facets during GaN pillar etching in Cl_2 plasma has been observed by other researchers [19,20,28]. In their work, Harrisson et al. [19] conducted a parametric study to investigate the influence of Cl_2/Ar plasma conditions (pressure, source ratio, etc.) on the GaN etch rate and pillar profile. They clearly observed the appearance of a-planes during the etching process for all plasma conditions except the ones showing limited etch selectivity with the hard mask. In this case, mask erosion at its edge led to striations along almost the entire height of the GaN pillar. However, facets were still visible at the bottom of the pillar. They attributed the formation of facets to a possible temperature effect that may increase the chemical component of the etch for long etching times. In our study, we excluded this hypothesis as the temperature process was checked with a temperature sticker attached to a sapphire wafer. Even after long processing times of 2000 seconds, the temperature was still in the range of 71-77 °C, slightly surpassing the chuck temperature of 55 °C. We suggest that the formation of facets is inherent to the etch mechanisms

of GaN in Cl_2 plasma. However, it is true that temperature, which generally enhances the chemical component of the etch, can facilitate facet formation.

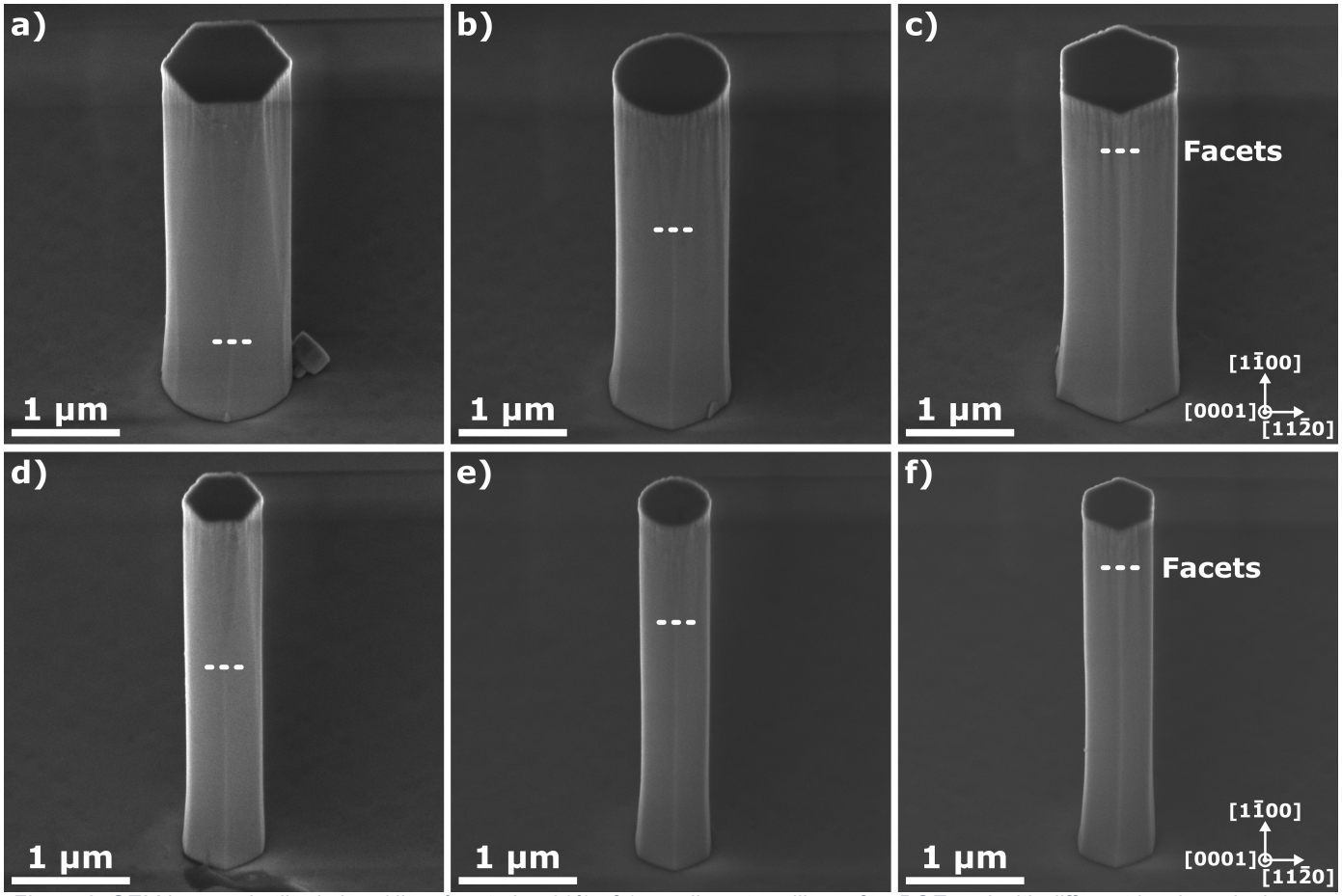

Figure 8. SEM images in tilted view (tilt 45°, rotation 30°) of 1 µm diameter pillars after BOE and with different hard mask shapes: a) hexagonal m-oriented, b) hexagonal a-oriented, c) circular. d), e), f) similar images on pillars of 0.5 µm diameter, the dashed line represents the height reached by the a-oriented facets.

Another interesting observation is the formation of hexagonal pits on the horizontal GaN surface during etching, which can be seen when the GaN is not entirely etched (cf. Fig. 9-a). In this case, the facets of the hexagonal V-pits correspond to m-type semipolar planes, such as (1-10k) planes. Similar defects with crystallographic orientation were observed during the KOH wet etching of (0001) GaN surface [31], as well as during (0001) GaN surface exposure to unbiased Cl_2 plasma, where the chemical component of the etching is enhanced [32]. Under such chemical-driven etching conditions, the c-plane GaN surfaces are very stable planes to etch, and the etching begins at the defective region of the GaN, namely along the dislocation pits. In their KOH wet study, Lai et al. observed that m-type semipolar planes appeared in the dislocation pit, first (1-102) planes that rapidly disappear to turn into (1-101) planes [31]. These planes persisted throughout the wet processing time until the GaN/sapphire interface was reached. At this point, lateral etching dominated, and the (1-101) planes were laterally consumed, and the etch stopped on m-nonpolar (1-100) planes. The origin of the m-oriented hexagonal pits in our study may follow similar mechanisms as those proposed for wet KOH. However, in our case, the etching of the GaN c-plane is activated by the ionic bombardment, as discussed in the next section.

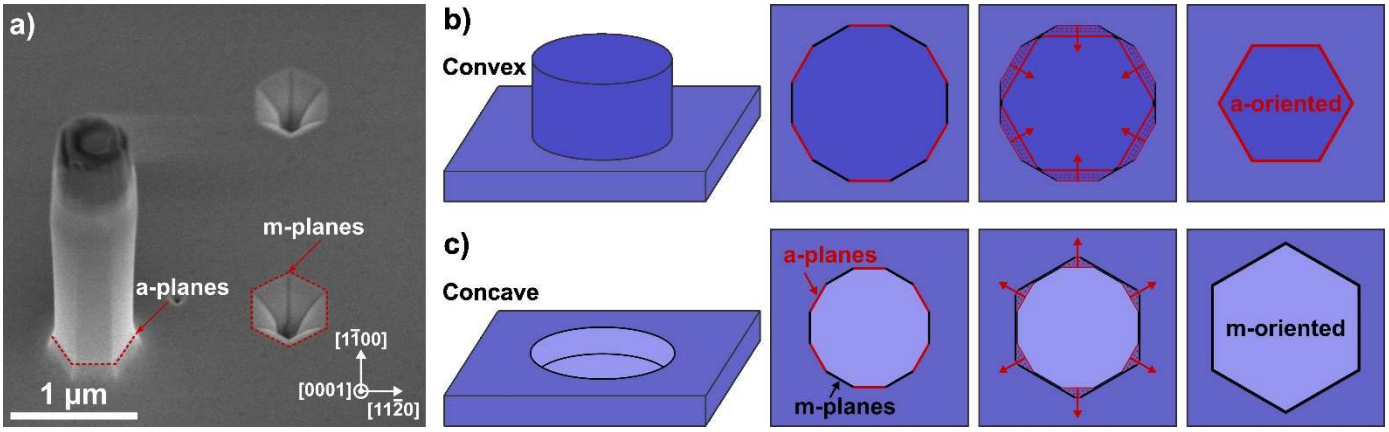

Figure 9. a) SEM images of a GaN sample partially etch where V-pits defect with m-type semi-polar planes are visible (tilt 30°, no rotation). b) and c) behaviour of convex and concave structures under chemical preferential etching where a-planes are etch faster than m-planes. The arrow indicate the etching direction.

3.3. Discussion on the orientation preferential etching of GaN in Cl_2 plasma

The mechanism for the wet etch of GaN by alkaline solutions assumes the oxidation of the gallium (Ga) atoms via hydroxide (OH^-) molecules attacking and breaking the Ga–N bonds, freeing the Ga atom to oxidize into Ga_2O_3 which is then dissolved [31,33,34].

$$2GaN + 3H_2O \xrightarrow{OH^-} Ga_2O_3 + 2NH_3$$

Equation 1. GaN etching mechanism in KOH solution [33,34]

Li et al [33] discovered that the surface's dangling bond configuration of N is essential to understanding selective etching on polar GaN surfaces. The fewer the nitrogen dangling bonds on a plane, the less steric hindrance for the OH− ions to attack the Ga-N bonds and bond with the Ga, resulting in a higher etch rate. Lai et al [31] refined Li et al's assumption and proposed calculating what they called the etching barrier index (EBI), defined as the planar atomic density of the crystallographic plane multiplied by the number of dangling bonds per nitrogen atom on that plane to describe the etching ability of a plane. Therefore, the higher the EBI value, the more challenging it is to etch a particular plane. From their calculation and Kazanowska's ones [28], the EBI of planes decreases as follows: c-polar plane > m-nonpolar plane > a-nonpolar plane > m-type semipolar plane (1-10k) k > 0 > a-type semipolar plane (11-2k) k > 0.

This classification implies that in a chemically driven etching regime, semipolar planes are etched faster than nonpolar ones and faster than c-planes, and globally, a-type planes are etched faster than m-type planes. This theory is highly consistent with experimental observations of GaN etching in KOH [35–37]. One consequence is that the slowest etching planes are the planes revealed by crystallographic etching and, therefore, wet etching. The facet with a high EBI usually becomes an etching stop and appears in the etching process.

However, other factors also influence the appearance of one plane over another: the local vertical etch rate versus the lateral etch rate, combined with the surface curvature (concave or convex that will be formed) [36,38]. It is observed that for a convex surface, fast etch facets persist, while for a concave surface, slow etch facets persist.

Based on all those mechanisms proposed for wet etching, we can propose the following mechanism for the preferential appearance for a-type plane on the pillar and m-type plane for the pits.

Using all the mechanisms proposed for wet etching, we can suggest the following mechanism to explain why a-type planes tend to appear more often on the pillars and m-type planes on the pits. Other publications

dealing with the etching of GaN in Cl_2 based plasma suggest that reactive chlorine preferentially reacts with Ga over N to form the volatile $GaCl_3$ compound, resulting in N-depleted GaN surfaces being observed [32]. Similar to the wet etch mechanisms in alkaline solution, the attack of Ga atoms by Cl may depend on the planar density and the N dangling bonds present on the plane. Based on this assumption and following the wet mechanisms exposed above, it is predicted that a-type planes will be chemically etched faster in Cl_2 based plasma. Of course, the difference with wet etching is that with plasma, the chemical component of the etch is enhanced by ion bombardment. However, Coulon's work [18] confirms that a similar trend is observed in an ion-enhanced chemical etching regime: a-semipolar planes are etched faster than a nonpolar plane and faster than polar c planes, regardless of the Cl_2 plasma conditions used. Considering that GaN etching is dominated by the chemical component, preferential crystallographic orientation can appear during the etch. Consistent with the wet etch mechanisms, we observe that in the pits that present concave surfaces with respect to the radical fluxes, the slow etch facets (m-type planes) form (cf. Fig. 9-c), while in the pillar that shows concave surfaces with respect to the radical fluxes, the fast etch facets (a-type planes) appear (cf. Fig. 9-b).

4. Conclusions

In the realm of optoelectronics and photonics, GaN-based nanostructures are of great interest due to their potential to access non-polar and semipolar crystal planes, which can significantly improve the light extraction and absorption of optoelectronic devices. However, achieving controlled fabrication of GaN nanostructures with specific crystallographic facets and final shapes is a challenging task. This study demonstrates that a top-down approach that combines lithography and Cl_2-based plasma etching can be used to transfer patterns while revealing smooth nonpolar facets. Although the etching of GaN in Cl_2 is driven by ion-enhanced chemical etching mechanisms, the chemical component is dominant, and the mechanisms that lead to facet formation are similar to those involved in wet KOH etching. Cl_2 plasma preferentially etches the nonpolar planes, but the final revealed plane depends on the surface curvature. Therefore, etching convex surfaces results in a-oriented facets, while concave surfaces result in m-plane facets. Even by changing the initial hard mask (HM) shape and orientation with respect to the GaN planes, it is difficult to reverse this trend. Although hexagonal or circular HM leads to a-oriented facet formation, an initial HM shape closer to the GaN a-plane will result in smooth facets from top to bottom, provided that the ion bombardment is well-controlled. However, top-down patterning using Cl_2-based plasma is not sufficient to produce m-oriented facets on pillars. Therefore, the fabrication of core-shell light-emitting structures requires an additional wet treatment after plasma patterning to reveal the intended m-oriented pillars. Previous studies [39,40] have shown the possibility of achieving m-plane faceting on GaN through wet treatments such as KOH. Our ongoing studies indeed confirm that by combining Cl_2 plasma etching of GaN pillars with an m-oriented hard mask, followed by a wet KOH treatment, well-defined m-plane facets can be obtained. The success of this strategy relies on the slope obtained after plasma etching.

This research was funded by the *French National Research Agency* in the framework of the program ANR-22-CE51-0032-01 and the *French National Research Agency* in the framework of the *"Investissements d'avenir"* program (ANR-15-IDEX-02). It was also supported by the French RENATECH network.

[1] H. Amano, R. Collazo, C.D. Santi, S. Einfeldt, M. Funato, J. Glaab, S. Hagedorn, A. Hirano, H. Hirayama, R. Ishii, Y. Kashima, Y. Kawakami, R. Kirste, M. Kneissl, R. Martin, F. Mehnke, M. Meneghini, A. Ougazzaden, P.J. Parbrook, S. Rajan, P. Reddy, F. Römer, J. Ruschel, B. Sarkar, F. Scholz, L.J. Schowalter, P. Shields, Z. Sitar, L. Sulmoni, T. Wang, T. Wernicke, M. Weyers, B. Witzigmann, Y.-R. Wu, T. Wunderer, Y. Zhang, The 2020 UV emitter roadmap, J. Phys. D: Appl. Phys. 53 (2020) 503001. https://doi.org/10.1088/1361-6463/aba64c.

[2] A. Waag, X. Wang, S. Fündling, J. Ledig, M. Erenburg, R. Neumann, M. Al Suleiman, S. Merzsch, J. Wei, S. Li, H.H. Wehmann, W. Bergbauer, M. Straßburg, A. Trampert, U. Jahn, H. Riechert, The nanorod approach: GaN NanoLEDs for solid state lighting, Phys. Status Solidi C. 8 (2011) 2296–2301. https://doi.org/10.1002/pssc.201000989.

[3] S. Li, A. Waag, GaN based nanorods for solid state lighting, Journal of Applied Physics. 111 (2012) 071101. https://doi.org/10.1063/1.3694674.

[4] H. Sekiguchi, K. Kishino, A. Kikuchi, Emission color control from blue to red with nanocolumn diameter of InGaN/GaN nanocolumn arrays grown on same substrate, Appl. Phys. Lett. 96 (2010) 231104. https://doi.org/10.1063/1.3443734.

[5] Q. Li, J.J. Figiel, G.T. Wang, Dislocation density reduction in GaN by dislocation filtering through a self-assembled monolayer of silica microspheres, Appl. Phys. Lett. 94 (2009) 231105. https://doi.org/10.1063/1.3152012.

[6] Y. Ra, S. Kang, C. Lee, Ultraviolet Light-Emitting Diode Using Nonpolar AlGaN Core–Shell Nanowire Heterostructures, Advanced Optical Materials. 6 (2018) 1701391. https://doi.org/10.1002/adom.201701391.

[7] Y. Zhao, H. Fu, G.T. Wang, S. Nakamura, Toward ultimate efficiency: progress and prospects on planar and 3D nanostructured nonpolar and semipolar InGaN light-emitting diodes, Adv. Opt. Photon. 10 (2018) 246–308. https://doi.org/10.1364/AOP.10.000246.

[8] R. Koester, J.-S. Hwang, D. Salomon, X. Chen, C. Bougerol, J.-P. Barnes, D.L.S. Dang, L. Rigutti, A. de Luna Bugallo, G. Jacopin, M. Tchernycheva, C. Durand, J. Eymery, M-Plane Core–Shell InGaN/GaN Multiple-Quantum-Wells on GaN Wires for Electroluminescent Devices, Nano Lett. 11 (2011) 4839–4845. https://doi.org/10.1021/nl202686n.

[9] C. Durand, C. Bougerol, J.-F. Carlin, G. Rossbach, F. Godel, J. Eymery, P.-H. Jouneau, A. Mukhtarova, R. Butté, N. Grandjean, *M*-Plane GaN/InAlN Multiple Quantum Wells in Core–Shell Wire Structure for UV Emission, ACS Photonics. 1 (2014) 38–46. https://doi.org/10.1021/ph400031x.

[10] M. Djavid, Z. Mi, Enhancing the light extraction efficiency of AlGaN deep ultraviolet light emitting diodes by using nanowire structures, Appl. Phys. Lett. 108 (2016) 051102. https://doi.org/10.1063/1.4941239.

[11] M. Monavarian, A. Rashidi, D. Feezell, A Decade of Nonpolar and Semipolar III-Nitrides: A Review of Successes and Challenges, Phys. Status Solidi A. (2018) 1800628. https://doi.org/10.1002/pssa.201800628.

[12] C.-C. Pan, S. Tanaka, F. Wu, Y. Zhao, J.S. Speck, S. Nakamura, S.P. DenBaars, D. Feezell, High-Power, Low-Efficiency-Droop Semipolar (20-2-1) Single-Quantum-Well Blue Light-Emitting Diodes, Appl. Phys. Express. 5 (2012) 062103. https://doi.org/10.1143/APEX.5.062103.

[13] T. Onuma, H. Amaike, M. Kubota, K. Okamoto, H. Ohta, J. Ichihara, H. Takasu, S.F. Chichibu, Quantum-confined Stark effects in the m-plane $In_{0.15}Ga_{0.85}N$⁄GaN multiple quantum well blue light-emitting diode fabricated on low defect density freestanding GaN substrate, Appl. Phys. Lett. 91 (2007) 181903. https://doi.org/10.1063/1.2802042.

[14] M. Yoshizawa, A. Kikuchi, M. Mori, N.F. Nobuhiko Fujita, K.K. Katsumi Kishino, Growth of Self-Organized GaN Nanostructures on $Al_2 O_3$ (0001) by RF-Radical Source Molecular Beam Epitaxy, Jpn. J. Appl. Phys. 36 (1997) L459. https://doi.org/10.1143/JJAP.36.L459.

[15] E. Calleja, M.A. Sánchez-García, F.J. Sánchez, F. Calle, F.B. Naranjo, E. Muñoz, U. Jahn, K. Ploog, Luminescence properties and defects in GaN nanocolumns grown by molecular beam epitaxy, Phys. Rev. B. 62 (2000) 16826–16834. https://doi.org/10.1103/PhysRevB.62.16826.

[16] P. Shields, M. Hugues, J. Zúñiga-Pérez, M. Cooke, M. Dineen, W. Wang, F. Causa, D. Allsopp, Fabrication and properties of etched GaN nanorods, Phys. Status Solidi C. 9 (2012) 631–634. https://doi.org/10.1002/pssc.201100394.

[17] E.D. Le Boulbar, C.J. Lewins, D.W.E. Allsopp, C.R. Bowen, P.A. Shields, Fabrication of high-aspect ratio GaN nanostructures for advanced photonic devices, Microelectronic Engineering. 153 (2016) 132–136. https://doi.org/10.1016/j.mee.2016.03.058.
[18] P.-M. Coulon, P. Feng, T. Wang, P. Shields, Impact of Inductively Coupled Plasma Etching Conditions on the Formation of Semi-Polar (11-22) and Non-Polar (11-20) GaN Nanorods, Nanomaterials. 10 (2020) 2562. https://doi.org/10.3390/nano10122562.
[19] S.E. Harrison, L.F. Voss, A.M. Torres, C.D. Frye, Q. Shao, R.J. Nikolić, Ultradeep electron cyclotron resonance plasma etching of GaN, Journal of Vacuum Science & Technology A. 35 (2017) 061303. https://doi.org/10.1116/1.4994829.
[20] C.D. Frye, C.E. Reinhardt, S.B. Donald, L.F. Voss, S.E. Harrison, ICP etching of GaN microstructures in a Cl_2–Ar plasma with subnanometer-scale sidewall surface roughness, Materials Science in Semiconductor Processing. 144 (2022) 106564. https://doi.org/10.1016/j.mssp.2022.106564.
[21] G.W. Pickrell, A.M. Armstrong, A.A. Allerman, M.H. Crawford, C.E. Glaser, J. Kempisty, V.M. Abate, Investigation of dry-etch-induced defects in >600 V regrown, vertical, GaN, p-n diodes using deep-level optical spectroscopy, Journal of Applied Physics. 126 (2019) 145703. https://doi.org/10.1063/1.5110521.
[22] K. Zhang, T. Takahashi, D. Ohori, G. Cong, K. Endo, N. Kumagai, S. Samukawa, M. Shimizu, X. Wang, High-quality nanodisk of InGaN/GaN MQWs fabricated by neutral-beam-etching and GaN regrowth: towards directional micro-LED in top-down structure, Semicond. Sci. Technol. 35 (2020) 075001. https://doi.org/10.1088/1361-6641/ab8539.
[23] J. Ladroue, A. Meritan, M. Boufnichel, P. Lefaucheux, P. Ranson, R. Dussart, Deep GaN etching by inductively coupled plasma and induced surface defects, Journal of Vacuum Science & Technology A. 28 (2010) 1226–1233. https://doi.org/10.1116/1.3478674.
[24] C.D. Frye, S.B. Donald, C. Reinhardt, L.F. Voss, S.E. Harrison, Impact of carrier wafer on etch rate, selectivity, morphology, and passivation during GaN plasma etching, Journal of Vacuum Science & Technology A. 39 (2021) 053002. https://doi.org/10.1116/6.0001123.
[25] M. Tahhan, J. Nedy, S.H. Chan, C. Lund, H. Li, G. Gupta, S. Keller, U. Mishra, Optimization of a chlorine-based deep vertical etch of GaN demonstrating low damage and low roughness, Journal of Vacuum Science & Technology A: Vacuum, Surfaces, and Films. 34 (2016) 031303. https://doi.org/10.1116/1.4944054.
[26] D.S. Rawal, H. Arora, B.K. Sehgal, R. Muralidharan, Comparative study of GaN mesa etch characteristics in Cl_2 based inductively coupled plasma with Ar and BCl_3 as additive gases, Journal of Vacuum Science & Technology A: Vacuum, Surfaces, and Films. 32 (2014) 031301. https://doi.org/10.1116/1.4868616.
[27] S.A. Smith, C.A. Wolden, M.D. Bremser, A.D. Hanser, R.F. Davis, W.V. Lampert, High rate and selective etching of GaN, AlGaN, and AlN using an inductively coupled plasma, Appl. Phys. Lett. 71 (1997) 3631–3633. https://doi.org/10.1063/1.120463.
[28] B.A. Kazanowska, K.R. Sapkota, P. Lu, A.A. Talin, E. Bussmann, T. Ohta, B.P. Gunning, K.S. Jones, G.T. Wang, Fabrication and field emission properties of vertical, tapered GaN nanowires etched via phosphoric acid, Nanotechnology. 33 (2022) 035301. https://doi.org/10.1088/1361-6528/ac2981.
[29] N. Posseme, T. Chevolleau, O. Joubert, L. Vallier, N. Rochat, Etching of porous SiOCH materials in fluorocarbon-based plasmas, J. Vac. Sci. Technol. B. 22 (2004) 2772. https://doi.org/10.1116/1.1815316.
[30] X. Detter, R. Palla, I. Thomas-Boutherin, E. Pargon, G. Cunge, O. Joubert, L. Vallier, Impact of chemistry on profile control of resist masked silicon gates etched in high density halogen-based plasmas, Journal of Vacuum Science & Technology B: Microelectronics and Nanometer Structures Processing, Measurement, and Phenomena. 21 (2003) 2174–2183. https://doi.org/10.1116/1.1612932.
[31] Y.-Y. Lai, S.-C. Hsu, H.-S. Chang, Y.S. Wu, C.-H. Chen, L.-Y. Chen, Y.-J. Cheng, The study of wet etching on GaN surface by potassium hydroxide solution, Research on Chemical Intermediates. 43 (2017) 3563–3572. https://doi.org/10.1007/s11164-016-2430-1.
[32] T. Meyer, C. Petit-Etienne, E. Pargon, Influence of the carrier wafer during GaN etching in Cl_2 plasma, Journal of Vacuum Science & Technology A. 40 (2022) 023202. https://doi.org/10.1116/6.0001478.
[33] D. Li, M. Sumiya, S. Fuke, D. Yang, D. Que, Y. Suzuki, Y. Fukuda, Selective etching of GaN polar surface in potassium hydroxide solution studied by x-ray photoelectron spectroscopy, Journal of Applied Physics. 90 (2001) 4219–4223. https://doi.org/10.1063/1.1402966.

[34] M. Itoh, T. Kinoshita, C. Koike, M. Takeuchi, K. Kawasaki, Y. Aoyagi, Straight and Smooth Etching of GaN (1-100) Plane by Combination of Reactive Ion Etching and KOH Wet Etching Techniques, Jpn. J. Appl. Phys. 45 (2006) 3988–3991. https://doi.org/10.1143/JJAP.45.3988.
[35] N. Al Taradeh, E. Frayssinet, C. Rodriguez, F. Morancho, C. Sonneville, L.-V. Phung, A. Soltani, F. Tendille, Y. Cordier, H. Maher, Characterization of m-GaN and a-GaN Crystallographic Planes after Being Chemically Etched in TMAH Solution, Energies. 14 (2021) 4241. https://doi.org/10.3390/en14144241.
[36] D.A. Stocker, E.F. Schubert, J.M. Redwing, Crystallographic wet chemical etching of GaN, Appl. Phys. Lett. 73 (1998) 2654–2656. https://doi.org/10.1063/1.122543.
[37] B. Leung, M.-C. Tsai, G. Balakrishnan, C. Li, S.R. Brueck, J.J. Figiel, P. Lu, G.T. Wang, Highly Anisotropic Crystallographic Etching for Fabrication of High-Aspect Ratio GaN Nanostructures., Sandia National Lab.(SNL-NM), Albuquerque, NM (United States), 2016.
[38] B.W. Batterman, Hillocks, Pits, and Etch Rate in Germanium Crystals, Journal of Applied Physics. 28 (1957) 1236–1241. https://doi.org/10.1063/1.1722624.
[39] Q. Li, K.R. Westlake, M.H. Crawford, S.R. Lee, D.D. Koleske, J.J. Figiel, K.C. Cross, S. Fathololoumi, Z. Mi, G.T. Wang, Optical performance of top-down fabricated InGaN/GaN nanorod light emitting diode arrays, Opt. Express. 19 (2011) 25528. https://doi.org/10.1364/OE.19.025528.
[40] Q. Li, J.B. Wright, W.W. Chow, T.S. Luk, I. Brener, L.F. Lester, G.T. Wang, Single-mode GaN nanowire lasers, Opt. Express. 20 (2012) 17873. https://doi.org/10.1364/OE.20.017873.